Negatively enhanced thermopower near a Van Hove singularity in electron-doped Sr_2RuO_4

Rei Nishinakayama,[1,*] Yoshiki J. Sato,[1,†] Takayoshi Yamanaka,[2] Yoshiteru Maeno,[3] Hiroshi Yaguchi,[1] Naoki Kikugawa,[4] and Ryuji Okazaki[1,‡]

[1]*Department of Physics and Astronomy, Tokyo University of Science, Noda 278-8510, Japan*
[2]*Institute for Materials Research, Tohoku University, Sendai 980-8577, Japan*
[3]*Toyota Riken-Kyoto University Research Center (TRiKUC), Kyoto 606-8501, Japan*
[4]*National Institute for Materials Science, Tsukuba 305-0003, Ibaraki, Japan*

(Received 28 November 2023; revised 14 April 2024; accepted 16 April 2024; published 31 May 2024)

The layered perovskite Sr_2RuO_4 serves as a model material of the two-dimensional (2D) Fermi liquid but also exhibits various emergent phenomena including the non-Fermi-liquid (NFL) behavior under external perturbations such as uniaxial pressure and chemical substitutions. Here we present the thermoelectric transport of electron-doped system $Sr_{2-y}La_yRuO_4$, in which a filling-induced Lifshitz transition occurs at the Van Hove singularity (VHS) point of $y \approx 0.2$. We find that the sign of the low-temperature thermopower becomes negative only near the VHS point, where the NFL behavior has been observed in the earlier study. This observation is incompatible with either a numerical calculation within a constant relaxation-time approximation or a toy-model calculation for the 2D Lifshitz transition adopting an elastic carrier scattering. As a promising origin of the observed negatively enhanced thermopower, we propose a skewed NFL state, in which an inelastic scattering with a considerable odd-frequency term plays a crucial role to negatively enhance the thermopower.

DOI: 10.1103/PhysRevResearch.6.023222

I. INTRODUCTION

Beyond the well-established Fermi-liquid (FL) picture, non-Fermi-liquid (NFL) state has been intensively investigated as an essential concept for various quantum phenomena [1–7]. Besides the well-known Tomonaga-Luttinger liquid in one dimension, the prototypical NFL state appears in a vicinity of the quantum critical point (QCP), in which a thermodynamic phase transition into an ordered state is suppressed by tuning external parameters. In the NFL state near QCP, the finite-temperature properties such as the electronic specific heat and the electrical resistivity drastically deviate from the FL behavior, as widely seen in correlated metals including transition-metal oxides and heavy fermions.

A yet unsolved, fundamental issue is how the FL picture is modified in a vicinity of the Lifshitz transition [8], an electronic topological transition associated with the change in the topology of the Fermi surfaces. The Lifshitz transition itself is ubiquitous; it is driven by various parameters such as pressure [9–11], magnetic field [12–15], band filling [16–18], and even temperature through the temperature-dependent chemical potential [19–22]. In spite of many observed examples, the kinetic properties near the Lifshitz transition are complex and still controversial owing to a peculiar energy-dependent relaxation time [23,24], which should become more complicated in correlated metals.

To tackle this problem, here we focus on the quasi-two-dimensional (q-2D) FL material Sr_2RuO_4 [25–28]. Indeed, its q-2D Fermi surfaces consisting of hole-like α and electron-like β and γ sheets have been accurately verified by the dHvA and the ARPES experiments [29–32]. The calculated Fermi surfaces of Sr_2RuO_4 are shown in Fig. 1(a). The normal-state nature in such a q-2D multiband system is well understood within the FL picture [26,33,34], whereas the pairing mechanism of the superconducting state is still an unsolved issue [35–39]. Significantly, its superconducting transition temperature T_c is enhanced to $T_c \approx 3.5$ K under compressional stress [40–43], and near the critical compression point in which T_c has a maximum value. Such variation of T_c corresponds to the sharp peak in the density of states (DOS) associated with a Van Hove singularity (VHS) point; such a topology change in the γ band is indeed observed by the ARPES [44]. Most importantly, the resistivity clearly deviates from the FL behavior near the VHS point [45,46], and also nontrivial electronic states such as entropic anomaly [47] have been observed near the Lifshitz transition [48–50]. Thus, this layered material offers a suitable platform to investigate the NFL nature near the Lifshitz transition.

In this paper, we report a thermopower study of the electron-doped system $Sr_{2-y}La_yRuO_4$ [51–53], in which a filling-induced Lifshitz transition occurs near the critical concentration $y_c \approx 0.2$ [31]. The calculated Fermi surfaces for

*6222526@alumni.tus.ac.jp
†Present address: Graduate School of Science and Engineering, Saitama University, Saitama 338-8570, Japan; yoshikisato@mail.saitama-u.ac.jp
‡okazaki@rs.tus.ac.jp

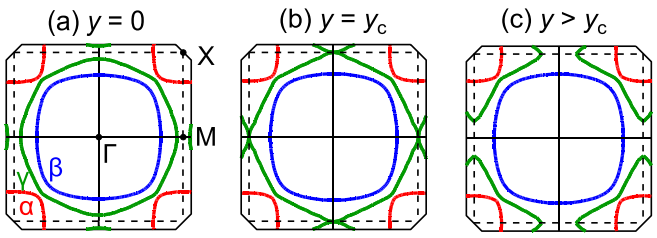

FIG. 1. The cross-sectional view of the calculated Fermi surfaces of $Sr_{2-y}La_yRuO_4$ at $k_z = 0$ plane for (a) $y = 0$, (b) $y = y_c$, and (c) $y > y_c$, drawn by using FermiSurfer program [63].

$y = y_c$ and $y > y_c$ are depicted in Figs. 1(b) and 1(c), respectively; the topology of the γ sheet changes at $y = y_c$. In $Sr_{2-y}La_yRuO_4$, similar electronic features including NFL transport [51] and the effective mass enhancement [31] have been clearly observed near $y = 0.2$, offering a complementary approach toward such an intriguing issue on the Lifshitz transition. We find that the low-temperature thermopower depends on the La content y and that the sign of the thermopower becomes negative only near the VHS point. This is in contrast to the results of the Hall effect measurements in which the Hall coefficient exhibits no significant anomaly near y_c [52]. We also show that the present experimental results cannot be explained either by numerical calculation results within a constant relaxation-time approximation or by a simple model for the 2D neck-disruption-type Lifshitz transition with an elastic carrier scattering. Instead, we propose a skewed NFL state [54] as a promising explanation for our results, in which an odd-frequency inelastic scattering is considered. The skewed NFL state is indeed a unique state of matter, as it has been studied as a nature of strange metal in cuprate superconductors and may also have a relevance to the transport properties in twisted bilayer graphene [54]. This skewed NFL state strengthens the electron-hole asymmetry owing to the dominant odd-frequency term in the scattering rate, providing a crucial role for negatively enhanced thermopower near the Lifshitz transition.

II. EXPERIMENTAL

Single crystals of $Sr_{2-y}La_yRuO_4$ were grown by a floating-zone method [51–53]. Typical dimension of the single crystals is $3 \times 1 \times 0.1$ mm^3. The in-plane thermopower was measured by a steady-state technique using a manganin-constantan differential thermocouple in a closed-cycle refrigerator [55,56]. A typical temperature gradient of 0.5 K/mm, which is adjusted along with the bath temperature, was applied along the in-plane direction using a resistive heater and the distance between the thermocouple contacts is about 1 mm. The thermoelectric voltage from the wire leads was subtracted.

III. RESULTS AND DISCUSSION

Figure 2(a) shows the temperature dependence of the in-plane thermopower S of $Sr_{2-y}La_yRuO_4$. It is known that T_c decreases with La substitution and is completely suppressed for y greater than 0.04 [51]. For the parent compound, the

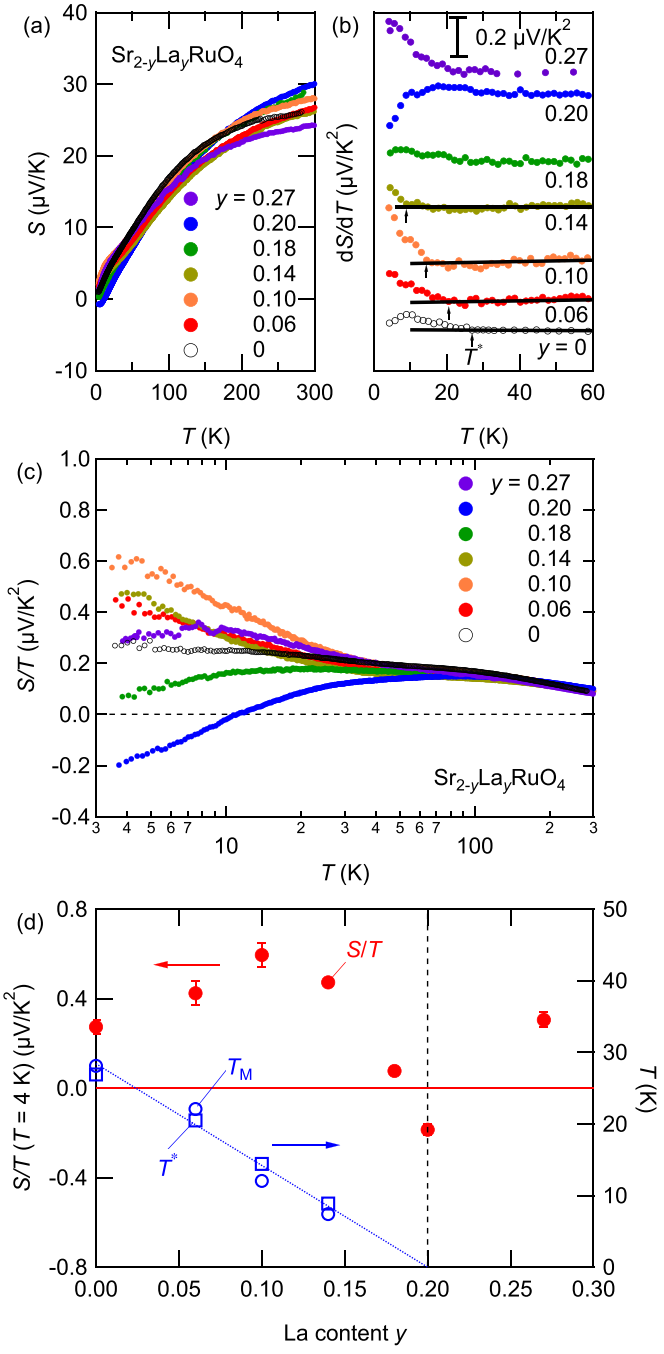

FIG. 2. (a) Temperature dependence of the thermopower S of $Sr_{2-y}La_yRuO_4$ ($0 \leqslant y \leqslant 0.27$) measured along the ab plane direction. (b) Temperature dependence of dS/dT. The arrows show the characteristic temperature T^* below which the dS/dT deviates from the linear temperature dependence of dS/dT at higher temperatures. The data are shifted vertically for clarity. (c) Temperature dependence of S/T. (d) The La content y dependence of S/T measured at 4 K (solid circles, left axis), T^* (open squares, right axis), and T_M (open circles, right axis). T_M is defined at the peak temperature in the magnetic susceptibility [53]. The blue-dotted line is a guide to the eye to represent the y dependence of these characteristic temperatures. The vertical-dashed line show the critical La content y_c.

present results well agree with those of the thermopower in previous reports [56–60]. The thermopower of Sr_2RuO_4 has also been studied by the dynamical mean-field theory [61]. In

the La-substituted compounds, overall behavior of the thermopower is similar to that of the parent crystal.

The thermopower in Sr_2RuO_4 was analyzed in the differential form dS/dT [Fig. 2(b)] to examine a characteristic temperature, and an anomaly was found near $T^* \approx 25$ K, below which dS/dT increases with decreasing temperature [57]. Subsequently, through the Seebeck and the Nernst measurements, Xu *et al.* have suggested that the coherence is developed below T^* [58]. As displayed in the right axis of Fig. 2(d), T^* systematically decreases with the La content y. It should be noted that the magnetic susceptibility of Sr_2RuO_4 is Pauli paramagnetic, but the temperature dependence exhibits a small peak structure at $T_M \approx 30$ K [26], below which the FL picture is well defined. The La content y dependence of T_M taken from Ref. [53] is also plotted in the right axis of Fig. 2(d). Notably, both T_M and T^* show similar y dependence, indicating that the characteristic temperature below which the coherence is formed in the correlated carriers decreases with increasing y. This trend is consistent with the NFL behavior near $y = 0.2$ [51] and also signifies the inherent role of the carrier scattering at the Lifshitz transition, as will be discussed later.

In Fig. 2(c), we also plot S/T of $Sr_{2-y}La_yRuO_4$ as a function of T. The low-temperature S/T behavior notably depends on both temperature and the La content y, suggesting the considerable change in the Fermi surfaces in the present La content range as reported in earlier reports [31,51–53]. It should be noted that negative thermopower is found at low temperatures only for the $y = 0.2$ crystal, which is near the critical La content y_c [31,51–53]. Figure 2(d) displays the La content y dependence of S/T obtained at 4 K for the left axis. With increasing y, S/T slightly increases and a singularity is clearly observed near $y \approx 0.2$. Note that a positive value of S/T is recovered at the higher content $y = 0.27$. To explain the observed La content dependence of S/T, we have examined the chemical potential dependence of S/T calculated within a constant relaxation-time approximation [62] (see Appendix), but the calculated data [Fig. 6(b)] is positively enhanced near the VHS points. Obviously, this discrepancy originates from the energy dependence of the relaxation time, which is ignored in the constant relaxation-time approximation method.

Here we discuss the energy dependence of the relaxation time $\tau(\varepsilon)$ near the Lifshitz transition. Similar to the case of Sr_2RuO_4, the 2D neck-disruption-type Lifshitz transition for the cylindrical Fermi surfaces [Fig. 3(a)] has been investigated [64–67]. In this case, the energy dependence of the DOS $D(\varepsilon)$ shows logarithmic divergence near the critical energy E_c at which the Lifshitz transition occurs [Fig. 3(b)]. Such logarithmic DOS behavior is also confirmed by the numerical calculation for Sr_2RuO_4 [Fig. 6(a) in Appendix]. Then, through an elastic impurity scattering, the scattering probability acquires a correction of the energy dependence of $1/\tau(\varepsilon) \propto D(\varepsilon)$ [23,24], which significantly affects the energy dependence of the conductivity function $\sigma(\varepsilon) \simeq D_0 v_0^2 \tau$. Note that the DOS D_0 and the velocity v_0 in this conductivity function exhibit weak-energy dependence because these mainly come from the electrons in the regular parts of the Fermi surfaces, which are far from the VHS points [68]. Figure 3(c) shows the calculated electrical conductivity for this simple model (see Appendix). The horizontal axis is the chemical

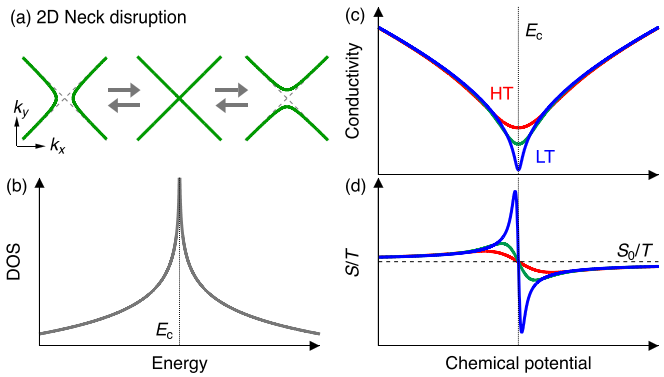

FIG. 3. 2D neck-disruption-type Lifshitz transitions and the physical properties. (a) The Fermi surface shape and (b) the DOS are symmetric around the critical energy E_c at which the Lifshitz transition occurs. (c) The conductivity and (d) the thermopower as a function of the chemical potential, which corresponds to the amount of electron doping by La substitution, for several temperatures. HT and LT represent high and low temperatures, respectively. The vertical-dotted lines show E_c and the horizontal-dashed line in (d) represents the contributions from the regular part of the Fermi surfaces, which is far from the VHS points.

potential and corresponds to the amount of electron doping by La substitution. As a consequence, the electrical conductivity σ decreases near E_c and such a modification leads to a NFL-like resistivity of $\rho(T) = \rho_0 + AT^n$ with $n < 2$ for Sr_2RuO_4 [46], as observed near the VHS point for both La-substituted [51] and uniaxially compressed [45] cases.

In this model, however, as shown in Fig. 3(d), the thermopower should exhibit positive and negative peaks with the same magnitudes below and above E_c, respectively [64–66], as indicated from the Mott formula [69]

$$\frac{S}{T} \propto -\frac{1}{\sigma}\frac{\partial\sigma}{\partial\varepsilon} \sim -\frac{1}{\tau}\frac{\partial\tau}{\partial\varepsilon}, \tag{1}$$

where the energy dependence of τ is crucial as similar to the case of the conductivity as mentioned before. It should be noted that such thermopower behavior with positive and negative peaks is also obtained in the numerical calculations for Sr_2RuO_4 in the elastic impurity scattering regime [46]. In contrast, for $Sr_{2-y}La_yRuO_4$, the low-temperature thermopower seems to be enhanced only negatively near the critical content $y_c \approx 0.2$ [Fig. 2(d)], which is difficult to explain with such a conventional neck disruption case. Also, as indicated in Fig. 2(d), an inelastic electron-electron scattering, not included in the model of Fig. 3, should be crucial near y_c.

To discuss the origin of the negatively enhanced thermopower near the VHS point, we next consider a phenomenological model adopting a skewed NFL state [54], in which an asymmetric inelastic scattering rate $1/\tau_{in} \propto (\pi T)^\nu g(\omega/T)$ characterized by a noneven scaling function $g(x) = |\Gamma(z)|^2 \cosh(x/2)/[\cosh(\alpha/2)\Gamma\{(1+\nu)/2\}^2]$ becomes essential, where $\Gamma(z)$ is the Γ function, $z = (1+\nu)/2 + i(x+\alpha)/2\pi$, $\omega = \varepsilon - \mu$ is a relative energy from the chemical potential μ, ν ($\leqslant 1$) is an exponent, and α is an parameter to induce the asymmetry in the scattering rate. Figure 4 shows the examples of a scaling function $g(\omega/T)$ with $\nu = 1$ for a symmetric (with an asymmetry parameter

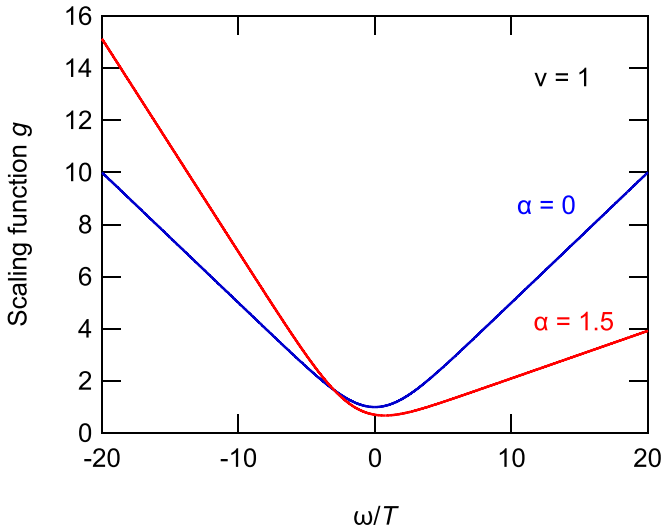

FIG. 4. Scaling function $g(\omega/T)$ for an exponent $\nu = 1$ and an asymmetry parameter $\alpha = 0$ and 1.5 [54]. The inelastic scattering rate $1/\tau_{\rm in}$ is given as $1/\tau_{\rm in} \propto (\pi T)^{\nu} g(\omega/T)$.

$\alpha = 0$) case and an asymmetric ($\alpha = 1.5$) case [54]. In the asymmetric case, owing to the odd-frequency term of the scattering rate, the contribution of either electrons or holes becomes stronger, and most importantly, the thermopower, a sensitive probe to the electron-hole asymmetry, is enhanced either negatively or positively. We infer that, along with the observation of the NFL resistivity near the VHS point [51], the observed negative sign of the thermopower may be a hallmark of such a skewed NFL state. Moreover, such unexpected sign change in the thermopower has also been discussed in the NFL regime of cuprate superconductors [70]. Note that the thermopower is also known as a sensitive probe for the entropic properties such as magnetic fluctuations but the present nonmagnetic system may not be adapted to such situation. At this stage, it is not easy to make a more quantitative calculation in this model, and further theoretical study is necessary to quantitatively account for the the sign change. Also, the frequency-dependent experiments such as the optical conductivity measurement will be crucial to examine the skewed NFL state.

Lifshitz transitions in correlated matter thus bring an intriguing issue on the NFL state. In this context, Sr_2RuO_4, in which a variety of electronic and magnetic states emerge under external perturbations [71–75], is of peculiar interest because it also exhibits the NFL behavior in Ti-substituted system [76]. Moreover, recent experimental and theoretical studies have revealed the appearance of enigmatic NFL states such as a Planckian metal characterized by a linear temperature dependence of the resistivity [77,78] and the quantum critical phase in frustrated materials [79,80], deepening underlying physics of the NFL state of matter.

IV. SUMMARY

In summary, we have measured the thermopower of the electron-doped system $Sr_{2-y}La_yRuO_4$ and observed an unusual sign change in the thermopower near the Lifshitz transition at the VHS point $y_c \approx 0.2$. We discuss the thermopower in a skewed NFL state, in which an asymmetric frequency dependence of the inelastic scattering rate is crucial, possibly leading to qualitative explanation for the negative sign of the thermopower near y_c. The present results thus offer a fascinating playground to investigate a variety of quantum phenomena of the correlated electrons near the Lifshitz transition.

ACKNOWLEDGMENTS

We appreciate Y. Fukumoto and R. Kurihara for discussion and R. Otsuki, H. Shiina, and R. Taira for the assistance. This work was partly supported by JSPS KAKENHI Grants No. 17H06136, No. 21H01033, No. 22H01166, No. 22H01168, and No. 22K19093.

APPENDIX

1. First-principles calculations

In order to investigate the thermopower theoretically, we performed first-principles calculations based on density functional theory (DFT) using Quantum Espresso [81–83]. We used the projector-augmented-wave pseudopotentials with the Perdew-Burke-Ernzerhof generalized-gradient-approximation (PBE-GGA) exchange-correlation functional. The cut-off energies for plane waves and charge densities were set to 70 and 560 Ry, respectively, and the k-point mesh was set to $20 \times 20 \times 20$ uniform grid to ensure the convergence. Using the obtained eigenvalues of the nth band at $\boldsymbol{k}$ point $E_{n,\boldsymbol{k}}$, the DOS $D(\varepsilon) = \sum_{n,\boldsymbol{k}} \delta(\varepsilon - E_{n,\boldsymbol{k}})$ was obtained using the optimized tetrahedron method [84], where δ is the delta function. We used on-site Coulomb energy $U = 3.5\,\text{eV}$ and exchange parameter $J = 0.6\,\text{eV}$ for Ru ions [85], and performed full relativistic calculations with spin-orbit coupling (DFT + U + SOC).

Figure 5(a) shows the calculated electronic band structure near the Fermi energy E_F of the parent material, which well coincides with the results in earlier studies [86–89]. The depicted k path is shown in Fig. 5(b). The β and γ bands at the high-symmetry points Γ and Z split owing to the inclusion of SOC [88], and the e_g bands are shifted upward due to the on-site U. The calculated DOS is depicted in Fig. 6(a), and the Van Hove singularity (VHS) point of the γ band to show the cusp anomaly is shifted slightly from $E \approx 50$ meV to $E \approx 30$ meV by including U + SOC. Such a trend is consistent with the results of ARPES experiment [31,32].

2. Calculated transport properties within a constant relaxation-time approximation

To examine the experimentally observed singular behavior in S/T, we have calculated the thermopower from the electronic band structure within the constant relaxation-time approximation. Note that the correlation effect of $4d$ electrons is considerable in Sr_2RuO_4 and the calculation results with local-density approximation are quantitatively different from the experimental observations [61]. On the other hand, the thermopower behavior in correlated metals is well described within a Fermi-liquid picture, where the correlation effect is included in the carrier effective mass [69]. Also, in

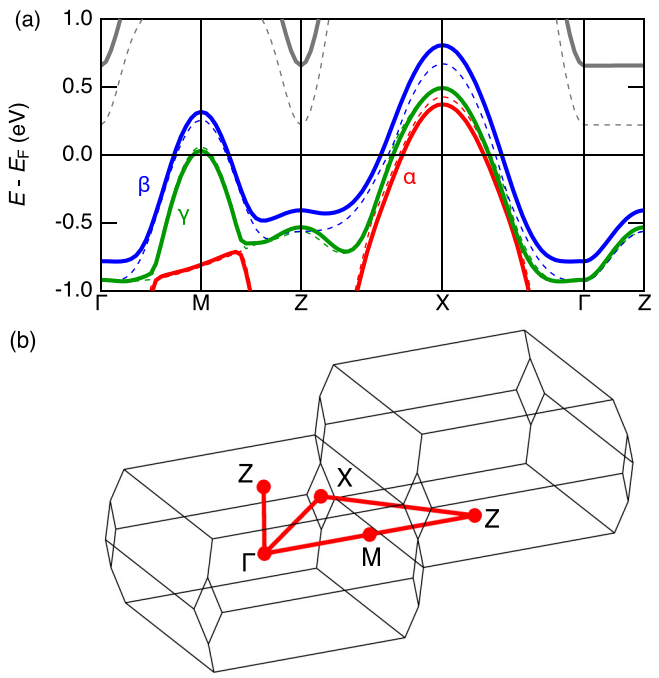

FIG. 5. (a) Calculated band structure of Sr_2RuO_4 with DFT + U + SOC scheme (solid curves). The dashed curves represent the results of scalar relativistic calculations and U is not included. The Van Hove singularity is at the M point, at which the γ band is slightly above E_F. (b) High-symmetry points in the Brillouin zone.

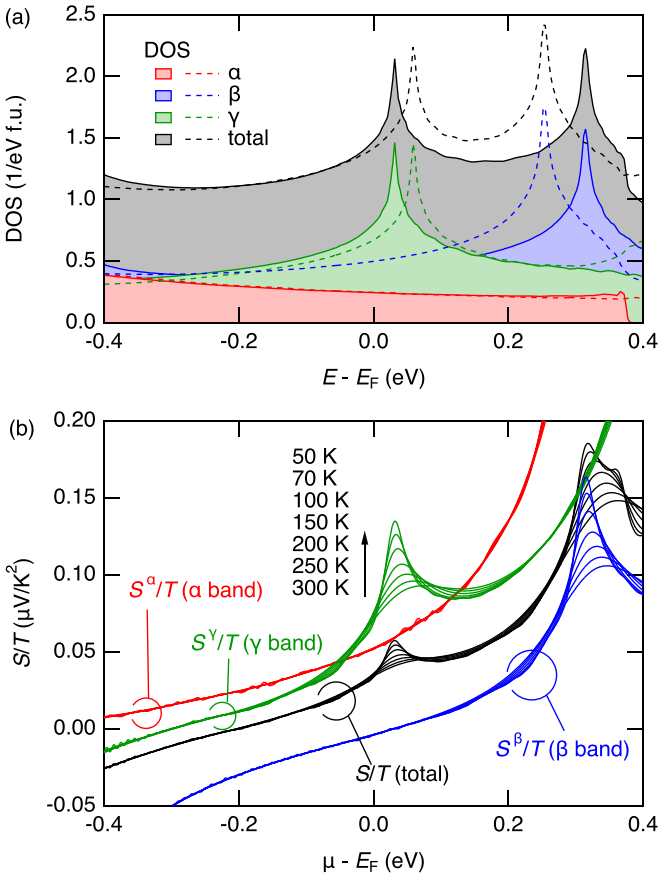

FIG. 6. (a) Calculated total and partial density of states with DFT + U + SOC scheme (solid-filled curves). The dashed curves represent the results of scalar relativistic calculations and U is not included. (b) Thermopower divided by temperature, S/T, calculated for several temperatures within the relaxation-time approximation. The horizontal axis shows the chemical potential measured from the Fermi energy of the parent compound. The black curves represent the total S/T and the red, blue, and green curves show the band-resolved data S^n/T for the α, β, and γ bands, respectively. Varying μ across the VHS results in the enhancement of the positive S/T.

$Sr_{2-y}La_yRuO_4$, the electron-doping effect by La substitution is well explained within a rigid band picture [31,51]. We thus examine how the band structure affects the thermopower.

The transport coefficients were calculated based on the linearized Boltzmann equations under constant relaxation-time approximation [62]. The transport distribution function tensor $L_{ij}(\varepsilon)$ is calculated as

$$L_{ij}(\varepsilon) = \sum_n L^n_{ij}(\varepsilon) = \sum_n \sum_{\mathbf{k}} v_i v_j \tau \delta(\varepsilon - E_{n,\mathbf{k}}), \qquad \text{(A1)}$$

where $L^n_{ij}(\varepsilon)$ is the partial transport distribution function tensor of the n-th band, v_i is the i-th component of the band velocity $\mathbf{v} = \frac{1}{\hbar}\nabla_{\mathbf{k}} E_{n,\mathbf{k}}$, and τ is the relaxation time. We calculated the partial electrical conductivity tensor of the n-th band of $\sigma^n_{ij}(\mu) = e^2 \int_{-\infty}^{\infty} d\varepsilon(-\frac{\partial f_0}{\partial \varepsilon}) L^n_{ij}$, where e is the elementary charge and f_0 is the Fermi-Dirac distribution function for the chemical potential μ and temperature T. The total electrical conductivity tensor is $\sigma_{ij}(\mu) = \sum_n \sigma^n_{ij}(\mu)$. Similarly, the partial Peltier conductivity tensor of nth band $P^n_{ij}(\mu) = [\sigma S]^n_{ij}(\mu)$ is

$$P^n_{ij}(\mu) = -\frac{e}{T}\int_{-\infty}^{\infty} d\varepsilon \left(-\frac{\partial f_0}{\partial \varepsilon}\right)(\varepsilon - \mu) L^n_{ij}, \qquad \text{(A2)}$$

where S_{ij} is the thermopower tensor. The total Peltier conductivity is given as $P_{ij}(\mu) = \sum_n P^n_{ij}(\mu)$. Hereafter we consider the in-plane component ($ij = aa$) only and the subscript will be omitted. The thermopower of the n-th band is then obtained as $S^n = P^n/\sigma^n$, and the total in-plane thermopower is given as $S = P/\sigma = \sum_n P^n / \sum_n \sigma^n$ as is generally seen in multiband systems.

Figure 6(b) depicts the thermopower divided by temperature, S/T, calculated for several temperatures within the constant relaxation-time approximation. The black curves represent the total S/T and the red, blue, and green curves show the band-resolved S^n/T for $n = \alpha$, β, γ, respectively. The horizontal axis is the chemical potential measured from the Fermi energy of the parent compound and corresponds to the amount of electron doping by La substitution. Note that the calculated values of S/T are significantly smaller than the experimental data because the electron correlation effect is not accurately included in this scheme and should be modified by using more precise methods such as the dynamical mean field theory [61]. Nevertheless, characteristic features reflecting the Lifshitz transition in Sr_2RuO_4 may be observed in the present calculations; the band-resolved S^n/T shows divergent behavior at low temperatures near 0.3 eV (β band) and 30 meV (γ band) corresponding to the VHS points of DOS for each band [Fig. 6(a)], while S^n/T exhibits almost no temperature dependence for the α band like a simple metal.

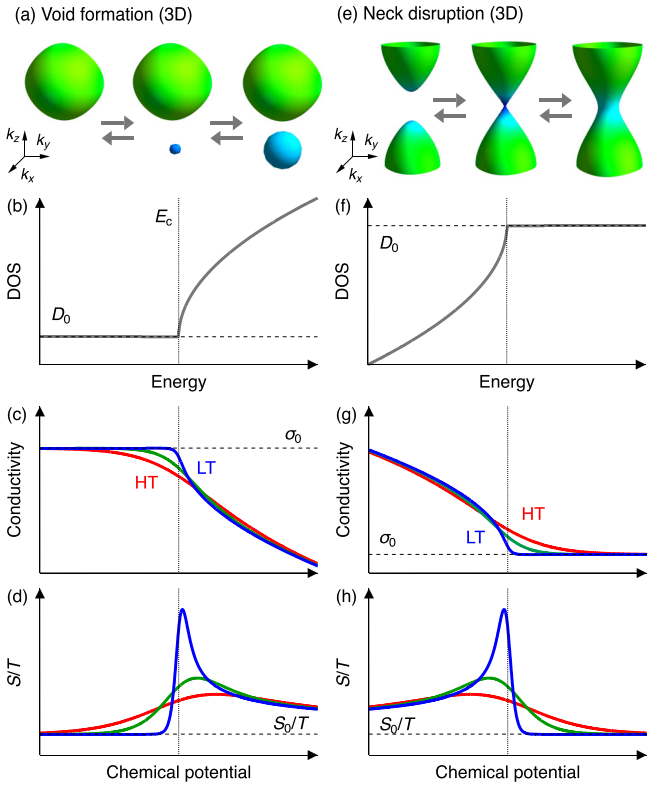

FIG. 7. Two types of the Lifshitz transitions for 3D case and the physical properties: (a)–(d) void formation and (e)–(h) neck disruption. For each panel, the dashed lines represent the contributions from the regular part of the Fermi surfaces. The vertical-dotted lines show the critical energy E_c at which the Lifshitz transition occurs. HT and LT represent high and low temperatures, respectively.

In general, the VHS points of DOS strongly affect the thermopower [90]. It is now important that the experimental data of S/T seems to negatively diverge near the critical concentration [Fig. 2(d) in the main text], while the calculated data is positively enhanced near the VHS points [Fig. 6(b)]. This discrepancy obviously originates from the energy dependence of the relaxation time ignored in the constant relaxation-time approximation.

3. Peculiar energy-dependent relaxation time and thermopower near the Lifshitz transition

Here we briefly review the three-dimensional (3D) case to see the significance of the scattering process. In the 3D case, the Lifshitz transition is categorized into two types of topological change in the Fermi surface called void formation and neck disruption, which are schematically shown in Figs. 7(a) and 7(e), respectively [8]. In the void formation case, for example, the DOS behaves as $D(\varepsilon) - D_0 \sim |\varepsilon - E_c|^{1/2}$, where D_0 is the DOS from the regular part of the Fermi surface (large void) and E_c is the critical energy above which a new void appears [Fig. 7(b)]. At first glance, such a small void with almost zero carrier velocity seems to give no contribution to the transport properties. Through the scattering process, however, electrons in the regular part exchange the momenta with those in the singular part (small void) and get virtually into the singular part [23,24,68]. As a result, according to the golden rule, the scattering probability acquires a correction of the energy dependence of $1/\tau(\varepsilon) \propto D(\varepsilon)$, and then the electrical conductivity $\sigma \propto \tau$ decreases above E_c [Fig. 7(c)]. Note that the energy dependence of τ is essential here as an approximate form $\sigma(\mu) \simeq e^2 \int_{-\infty}^{\infty} d\varepsilon(-\frac{\partial f_0}{\partial \varepsilon}) D v^2 \tau \simeq e^2 D_0 v_0^2 \tau(\mu)$, because the DOS D_0 and the velocity v_0 in the conductivity mainly come from the electrons in the large void [68].

According to the Mott formula, the thermopower S is given as

$$\frac{S}{T} \propto -\frac{1}{\sigma}\frac{\partial \sigma}{\partial \varepsilon} \sim -\frac{1}{\tau}\frac{\partial \tau}{\partial \varepsilon}, \tag{A3}$$

where the energy dependence of τ is crucial as similar to the case of the conductivity, and thus it shows a sharp peak structure at low temperatures [Fig. 7(d)]. The similar situation occurs in the case of the neck disruption [Figs. 7(e)–7(h)] and the thermopower is also enhanced positively near the critical point. Note that the singularities in σ and S are smeared with increasing temperature. These thermoelectric singularities in 3D case have been experimentally observed in the Li-Mg alloy [91].

4. Calculations of the transport properties for the Lifshitz transitions

Here we show the calculation details for the transport coefficients near the Lifshitz transition by using the energy-dependent scattering time. The electrical conductivity σ and the Peltier conductivity $P = \sigma S$ are given as

$$\begin{bmatrix} \sigma \\ P \end{bmatrix} = \begin{bmatrix} e^2 \\ -\frac{e}{T} \end{bmatrix} \int_{-\infty}^{\infty} d\varepsilon \left(-\frac{\partial f_0}{\partial \varepsilon}\right) \begin{bmatrix} 1 \\ \varepsilon - \mu \end{bmatrix} L \tag{A4}$$

$$= \frac{e}{4k_B T^2} \int_{-\infty}^{\infty} \frac{d\omega}{\cosh^2(\beta\omega/2)} \begin{bmatrix} eT \\ -\omega \end{bmatrix} L, \tag{A5}$$

where $\omega = \varepsilon - \mu$ is the relative energy measured from the chemical potential. Using the energy-dependent scattering time, the transport function near the Lifshitz transition is approximately given as

$$L = D_0 v_0^2 \tau(\varepsilon), \tag{A6}$$

and the transport coefficients are given as

$$\begin{bmatrix} \sigma \\ P \end{bmatrix} = \frac{e D_0 v_0^2}{4k_B T^2} \int_{-\infty}^{\infty} \frac{d\omega}{\cosh^2(\beta\omega/2)} \begin{bmatrix} eT \\ -\omega \end{bmatrix} \tau(\omega), \tag{A7}$$

where the scattering time is model dependent as described below.

For the 3D void formation case in Figs. 7(a)–7(d), the density of states is expressed as

$$D(\varepsilon) \sim D_0 + a|\varepsilon - E_c|^{1/2}\theta(\varepsilon - E_c), \tag{A8}$$

where a (> 0) is a constant and θ is the Heaviside step function, as is shown in Fig. 7(b). The scattering time is then given as

$$\tau(\varepsilon) \sim D(\varepsilon)^{-1} \tag{A9}$$

$$\sim D_0 - a|\varepsilon - E_c|^{1/2}\theta(\varepsilon - E_c) \tag{A10}$$

$$= D_0 - a|\omega + Z|^{1/2}\theta(\omega + Z), \tag{A11}$$

where $Z = \mu - E_c$ is the chemical potential measured from the critical energy. The transport coefficients are now calculated and the thermopower S is give as $S = P/\sigma$. Note that although the regular part D_0 also depends on the energy [23,24], the energy dependence of the singular part is much significant. Indeed, the calculation results shown in Fig. 7 are similar to the earlier studies.

For the 3D neck disruption case [Figs. 7(e)–7(h)], the scattering time is given as

$$\tau(\varepsilon) \sim D_0 + a|E_c - \varepsilon|^{1/2}\theta(E_c - \varepsilon) \tag{A12}$$

$$= D_0 + a|-\omega - Z|^{1/2}\theta(-\omega - Z), \tag{A13}$$

which is similar to the case of void formation.

For the symmetric 2D neck disruption case [Figs. 3(a)–3(d) in the main text], the density of states near the Lifshitz transition is given as a logarithmic form of

$$D(\varepsilon) \sim \ln \frac{t}{|\varepsilon - E_c|}, \tag{A14}$$

where t (> 0) is a constant as is shown in Fig. 3(b) in the main text. The scattering time is given as

$$\tau(\varepsilon) \sim \left(\ln \frac{t}{|\varepsilon - E_c|}\right)^{-1} = \left(\ln \frac{t}{|\omega + Z|}\right)^{-1}. \tag{A15}$$

[1] J. A. Hertz, Quantum critical phenomena, Phys. Rev. B **14**, 1165 (1976).

[2] A. J. Millis, Effect of a nonzero temperature on quantum critical points in itinerant fermion systems, Phys. Rev. B **48**, 7183 (1993).

[3] G. R. Stewart, Non-Fermi-liquid behavior in d- and f-electron metals, Rev. Mod. Phys. **73**, 797 (2001).

[4] H. v. Löhneysen, A. Rosch, M. Vojta, and Peter Wölfle, Fermi-liquid instabilities at magnetic quantum phase transitions, Rev. Mod. Phys. **79**, 1015 (2007).

[5] S. Sachdev, Quantum magnetism and criticality, Nat. Phys. **4**, 173 (2008).

[6] P. Gegenwart, Q. Si, and F. Steglich, Quantum criticality in heavy-fermion metals, Nat. Phys. **4**, 186 (2008).

[7] D. Chowdhury, A. Georges, O. Parcollet, and S. Sachdev, Sachdev-Ye-Kitaev models and beyond: Window into non-Fermi liquids, Rev. Mod. Phys. **94**, 035004 (2022).

[8] I. Lifshitz, Anomalies of electron characteristics of a metal in the high pressure region, Sov. Phys. JETP **11**, 1130 (1960).

[9] T. Nishimura, H. Sakai, H. Mori, K. Akiba, H. Usui, M. Ochi, K. Kuroki, A. Miyake, M. Tokunaga, Y. Uwatoko, K. Katayama, H. Murakawa, and N. Hanasaki, Large enhancement of thermoelectric efficiency due to a pressure-induced Lifshitz transition in SnSe, Phys. Rev. Lett. **122**, 226601 (2019).

[10] M. Krottenmüller, M. Vöst, N. Unglert, J. Ebad-Allah, G. Eickerling, D. Volkmer, J. Hu, Y. L. Zhu, Z. Q. Mao, W. Scherer, and C. A. Kuntscher, Indications for Lifshitz transitions in the nodal-line semimetal ZrSiTe induced by interlayer interaction, Phys. Rev. B **101**, 081108(R) (2020).

[11] S. Sen and G.-Y. Guo, Pressure induced Lifshitz transition in ThFeAsN, Phys. Rev. Mater. **4**, 104802 (2020).

[12] H. Pfau, R. Daou, S. Friedemann, S. Karbassi, S. Ghannadzadeh, R. Küchler, S. Hamann, A. Steppke, D. Sun, M. König, A. P. Mackenzie, K. Kliemt, C. Krellner, and M. Brando, Cascade of magnetic-field-induced Lifshitz transitions in the ferromagnetic Kondo lattice material $YbNi_4P_2$, Phys. Rev. Lett. **119**, 126402 (2017).

[13] D. Schulze Grachtrup, N. Steinki, S. Süllow, Z. Cakir, G. Zwicknagl, Y. Krupko, I. Sheikin, M. Jaime, and J. A. Mydosh, Magnetic phase diagram and electronic structure of UPt_2Si_2 at high magnetic fields: A possible field-induced Lifshitz transition, Phys. Rev. B **95**, 134422 (2017).

[14] A. Pourret, S. G. Sharapov, T. D. Matsuda, G. Knebel, G. Zwicknagl, and A. A. Varlamov, Transport spectroscopy of the field induced cascade of Lifshitz transitions in $YbRh_2Si_2$, J. Phys. Soc. Jpn. **88**, 104702 (2019).

[15] L. Wu, S. Chi, H. Zuo, G. Xu, L. Zhao, Y. Luo, and Z. Zhu, Field-induced Lifshitz transition in the magnetic Weyl semimetal candidate PrAlSi, npj Quantum Mater. **8**, 4 (2023).

[16] Y. Okamoto, A. Nishio, and Z. Hiroi, Discontinuous Lifshitz transition achieved by band-filling control in Na_xCoO_2, Phys. Rev. B **81**, 121102(R) (2010).

[17] J. Kwon, M. Kim, D. Song, Y. Yoshida, J. Denlinger, W. Kyung, and C. Kim, Lifshitz-transition-driven metal-insulator transition in moderately spin-orbit-coupled $Sr_{2-x}La_xRhO_4$, Phys. Rev. Lett. **123**, 106401 (2019).

[18] N. Ito, M. Ishii, and R. Okazaki, Enhanced Seebeck coefficient by a filling-induced Lifshitz transition in K_xRhO_2, Phys. Rev. B **99**, 041112(R) (2019).

[19] Y. Wu *et al.*, Temperature-induced Lifshitz transition in WTe_2, Phys. Rev. Lett. **115**, 166602 (2015).

[20] Y. Zhang *et al.*, Electronic evidence of temperature-induced Lifshitz transition and topological nature in $ZrTe_5$, Nat. Commun. **8**, 15512 (2017).

[21] F. C. Chen, Y. Fei, S. J. Li, Q. Wang, X. Luo, J. Yan, W. J. Lu, P. Tong, W. H. Song, X. B. Zhu, L. Zhang, H. B. Zhou, F. W. Zheng, P. Zhang, A. L. Lichtenstein, M. I. Katsnelson, Y. Yin, N. Hao, and Y. P. Sun, Temperature-induced Lifshitz transition and possible excitonic instability in ZrSiSe, Phys. Rev. Lett. **124**, 236601 (2020).

[22] Y. Tian, Y. Zhu, R. Li, Z. Mao, and J. H. Ross, Jr., NMR determination of Van Hove singularity and Lifshitz transitions in the nodal-line semimetal ZrSiTe, Phys. Rev. B **104**, L041105 (2021).

[23] A. A. Varlamov, V. S. Egorov, and A. V. Pantsulaya, Kinetic properties of metals near electronic topological transitions (2 1/2-order transitions), Adv. Phys. **38**, 469 (1989).

[24] A. A. Varlamov, Y. M. Galperin, S. G. Sharapov, and Y. Yerin, Concise guide for electronic topological transitions, Low Temp. Phys. **47**, 672 (2021).

[25] Y. Maeno, H. Hashimoto, K. Yoshida, S. Nishizaki, T. Fujita, J. G. Bednorz, and F. Lichtenberg, Superconductivity in a layered perovskite without copper, Nature (London) **372**, 532 (1994).

[26] A. P. Mackenzie and Y. Maeno, The superconductivity of Sr_2RuO_4 and the physics of spin-triplet pairing, Rev. Mod. Phys. **75**, 657 (2003).

[27] A. P. Mackenzie, T. Scaffidi, C. W. Hicks, and Y. Maeno, Even odder after twenty-three years: The superconducting order parameter puzzle of Sr_2RuO_4, npj Quant. Mater. **2**, 40 (2017).

[28] S. A. Kivelson, A. C. Yuan, B. Ramshaw, and R. Thomale, A proposal for reconciling diverse experiments on the superconducting state in Sr_2RuO_4, npj Quantum Mater. **5**, 43 (2020).

[29] A. P. Mackenzie, S. R. Julian, A. J. Diver, G. J. McMullan, M. P. Ray, G. G. Lonzarich, Y. Maeno, S. Nishizaki, and T. Fujita, Quantum oscillations in the layered perovskite superconductor Sr_2RuO_4, Phys. Rev. Lett. **76**, 3786 (1996).

[30] A. Damascelli, D. H. Lu, K. M. Shen, N. P. Armitage, F. Ronning, D. L. Feng, C. Kim, Z.-X. Shen, T. Kimura, Y. Tokura, Z. Q. Mao, and Y. Maeno, Fermi surface, surface states, and surface reconstruction in Sr_2RuO_4, Phys. Rev. Lett. **85**, 5194 (2000).

[31] K. M. Shen, N. Kikugawa, C. Bergemann, L. Balicas, F. Baumberger, W. Meevasana, N. J. C. Ingle, Y. Maeno, Z.-X. Shen, and A. P. Mackenzie, Evolution of the Fermi surface and quasiparticle renormalization through a Van Hove singularity in $Sr_{2-y}La_yRuO_4$, Phys. Rev. Lett. **99**, 187001 (2007).

[32] A. Tamai, M. Zingl, E. Rozbicki, E. Cappelli, S. Riccò, A. de la Torre, S. McKeown Walker, F. Y. Bruno, P. D. C. King, W. Meevasana, M. Shi, M. Radović, N. C. Plumb, A. S. Gibbs, A. P. Mackenzie, C. Berthod, H. U. R. Strand, M. Kim, A. Georges, and F. Baumberger, High-resolution photoemission on Sr_2RuO_4 reveals correlation-enhanced effective spin-orbit coupling and dominantly local self-energies, Phys. Rev. X **9**, 021048 (2019).

[33] D. Stricker, J. Mravlje, C. Berthod, R. Fittipaldi, A. Vecchione, A. Georges, and D. van der Marel, Optical response of Sr_2RuO_4 reveals universal Fermi-liquid scaling and quasiparticles beyond landau theory, Phys. Rev. Lett. **113**, 087404 (2014).

[34] C. Bergemann, A. P. Mackenzie, S. R. Julian, D. Forsythe, and E. Ohmichi, Quasi-two-dimensional Fermi liquid properties of the unconventional superconductor Sr_2RuO_4, Adv. Phys. **52**, 639 (2003).

[35] A. Pustogow, Y. Luo, A. Chronister, Y.-S. Su, D. A. Sokolov, F. Jerzembeck, A. P. Mackenzie, C. W. Hicks, N. Kikugawa, S. Raghu, E. D. Bauer, and S. E. Brown, Constraints on the superconducting order parameter in Sr_2RuO_4 from oxygen-17 nuclear magnetic resonance, Nature (London) **574**, 72 (2019).

[36] K. Ishida, M. Manago, K. Kinjo, and Y. Maeno, Reduction of the ^{17}O Knight shift in the superconducting state and the heat-up effect by NMR pulses on Sr_2RuO_4, J. Phys. Soc. Jpn. **89**, 034712 (2020).

[37] S. Benhabib, C. Lupien, I. Paul, L. Berges, M. Dion, M. Nardone, A. Zitouni, Z. Q. Mao, Y. Maeno, A. Georges, L. Taillefer, and C. Proust Ultrasound evidence for a two-component superconducting order parameter in Sr_2RuO_4, Nat. Phys. **17**, 194 (2021).

[38] S. Ghosh, A. Shekhter, F. Jerzembeck, N. Kikugawa, D. A. Sokolov, M. Brando, A. P. Mackenzie, C. W. Hicks, and B. J. Ramshaw, Thermodynamic evidence for a two-component superconducting order parameter in Sr_2RuO_4, Nat. Phys. **17**, 199 (2021).

[39] V. Grinenko, S. Ghosh, R. Sarkar, J.-C. Orain, A. Nikitin, M. Elender, D. Das, Z. Guguchia, F. Brückner, M. E. Barber *et al.*, Split superconducting and time-reversal symmetry-breaking transitions in Sr_2RuO_4 under stress, Nat. Phys. **17**, 748 (2021).

[40] C. W. Hicks, D. O. Brodsky, E. A. Yelland, A. S. Gibbs, J. A. N. Bruin, M. E. Barber, S. D. Edkins, K. Nishimura, S. Yonezawa, Y. Maeno, and A. P. Mackenzie, Strong increase of T_c of Sr_2RuO_4 under both tensile and compressive strain, Science **344**, 283 (2014).

[41] H. Taniguchi, K. Nishimura, S. K. Goh, S. Yonezawa, and Y. Maeno, Higher-T_c superconducting phase in Sr_2RuO_4 induced by in-plane uniaxial pressure, J. Phys. Soc. Jpn. **84**, 014707 (2015).

[42] A. Steppke, L. Zhao, M. E. Barber, T. Scaffidi, F. Jerzembeck, H. Rosner, A. S. Gibbs, Y. Maeno, S. H. Simon, A. P. Mackenzie, and C. W. Hicks, Strong peak in T_c of Sr_2RuO_4 under uniaxial pressure, Science **355**, eaaf9398 (2017).

[43] Y.-S. Li, N. Kikugawa, D. A. Sokolov, F. Jerzembeck, A. S. Gibbs, Y. Maeno, C. W. Hicks, J. Schmalian, M. Nicklas, and A. P. Mackenzie, High-sensitivity heat-capacity measurements on Sr_2RuO_4 under uniaxial pressure, Proc. Natl. Acad. Sci. U.S.A. **118**, e2020492118 (2021).

[44] V. Sunko, E. A. Morales, I. Marković, M. E. Barber, D. Milosavljević, F. Mazzola, D. A. Sokolov, N. Kikugawa, C. Cacho, P. Dudin, H. Rosner, C. W. Hicks, P. D. C. King, and A. P. Mackenzie, Direct observation of a uniaxial stress-driven Lifshitz transition in Sr_2RuO_4, npj Quantum Mater. **4**, 46 (2019).

[45] M. E. Barber, A. S. Gibbs, Y. Maeno, A. P. Mackenzie, and C. W. Hicks, Resistivity in the vicinity of a Van Hove singularity: Sr_2RuO_4 under uniaxial pressure, Phys. Rev. Lett. **120**, 076602 (2018).

[46] F. Herman, J. Buhmann, M. H. Fischer, and M. Sigrist, Deviation from Fermi-liquid transport behavior in the vicinity of a Van Hove singularity, Phys. Rev. B **99**, 184107 (2019).

[47] Y.-S. Li, M. Garst, J. Schmalian, S. Ghosh, N. Kikugawa, D. A. Sokolov, C. W. Hicks, F. Jerzembeck, M. S. Ikeda, Z. Hu, B. J. Ramshaw *et al.*, Elastocaloric determination of the phase diagram of Sr_2RuO_4, Nature (London) **607**, 276 (2022).

[48] Y. Luo, A. Pustogow, P. Guzman, A. P. Dioguardi, S. M. Thomas, F. Ronning, N. Kikugawa, D. A. Sokolov, F. Jerzembeck, A. P. Mackenzie, C. W. Hicks, E. D. Bauer, I. I. Mazin, and S. E. Brown, Normal state ^{17}O NMR studies of Sr_2RuO_4 under uniaxial stress, Phys. Rev. X **9**, 021044 (2019).

[49] E. A. Morales, G.-R. Siemann, A. Zivanovic, P. A. E. Murgatroyd, I. Markovic, B. Edwards, C. A. Hooley, D. A. Sokolov, N. Kikugawa, C. Cacho, M. D. Watson, T. K. Kim, C. W. Hicks, A. P. Mackenzie, and P. D. C. King, Hierarchy of Lifshitz transitions in the surface electronic structure of Sr_2RuO_4 under uniaxial compression, Phys. Rev. Lett. **130**, 096401 (2023).

[50] B. Kim, S. Khmelevskyi, C. Franchini, and I. I. Mazin, Suppressed fluctuations as the origin of the static magnetic order in strained Sr_2RuO_4, Phys. Rev. Lett. **130**, 026702 (2023).

[51] N. Kikugawa, A. P. Mackenzie, C. Bergemann, R. A. Borzi, S. A. Grigera, and Y. Maeno, Rigid-band shift of the Fermi level in the strongly correlated metal: $Sr_{2-y}La_yRuO_4$, Phys. Rev. B **70**, 060508(R) (2004).

[52] N. Kikugawa, A. P. Mackenzie, C. Bergemann, and Y. Maeno, Low-temperature Hall effect in substituted Sr_2RuO_4, Phys. Rev. B **70**, 174501 (2004).

[53] N. Kikugawa, C. Bergemann, A. P. Mackenzie, and Y. Maeno, Band-selective modification of the magnetic fluctuations in Sr_2RuO_4: A study of substitution effects, Phys. Rev. B **70**, 134520 (2004).

[54] A. Georges and J. Mravlje, Skewed non-Fermi liquids and the Seebeck effect, Phys. Rev. Res. **3**, 043132 (2021).

[55] N. Kouda, K. Eguchi, R. Okazaki, and M. Tamura, Anomalous scaling law for thermoelectric transport of two-dimension-confined electrons in an organic molecular system, Phys. Rev. Res. **4**, 043050 (2022).

[56] T. Yamanaka, R. Okazaki, and H. Yaguchi, Enhanced Seebeck coefficient through magnetic fluctuations in $Sr_2Ru_{1-x}M_xO_4$ (M = Co, Mn), Phys. Rev. B **105**, 184507 (2022).

[57] H. Yoshino, K. Murata, N. Shirakawa, Y. Nishihara, Y. Maeno, and T. Fujita, Thermopower of a layered perovskite superconductor, Sr_2RuO_4, J. Phys. Soc. Jpn. **65**, 1548 (1996).

[58] X. F. Xu, Z. A. Xu, T. J. Liu, D. Fobes, Z. Q. Mao, J. L. Luo, and Y. Liu, Band-dependent normal-state coherence in Sr_2RuO_4: Evidence from nernst effect and thermopower measurements, Phys. Rev. Lett. **101**, 057002 (2008).

[59] R. Daou, S. Hébert, G. Grissonnanche, E. Hassinger, L. Taillefer, H. Taniguchi, Y. Maeno, A. S. Gibbs, and A. P. Mackenzie, Anisotropic Seebeck coefficient of Sr_2RuO_4 in the incoherent regime, Phys. Rev. B **108**, L121106 (2023).

[60] R. Otsuki, Y. J. Sato, R. Okazaki, T. Komine, R. Kurihara, and H. Yaguchi, Carrier filtering effect for enhanced thermopower in a body-centered tetragonal ruthenate, Phys. Rev. Mater. **7**, 125401 (2023).

[61] J. Mravlje and A. Georges, Thermopower and entropy: Lessons from Sr_2RuO_4, Phys. Rev. Lett. **117**, 036401 (2016).

[62] G. K. H. Madsen, BoltzTraP. A code for calculating band-structure dependent quantities, Comput. Phys. Commun. **175**, 67 (2006).

[63] M. Kawamura, FermiSurfer: Fermi-surface viewer providing multiple representation schemes, Comput. Phys. Commun. **239**, 197 (2019).

[64] Y. M. Blanter, A. V. Pantsulaya, and A. A. Varlamov, Thermoelectric power and topological transitions in quasi-two-dimensional electronic systems, Phys. Rev. B **45**, 6267 (1992).

[65] Y. Yamaji, T. Misawa, and M. Imada, Quantum and topological criticalities of Lifshitz transition in two-dimensional correlated electron systems, J. Phys. Soc. Jpn. **75**, 094719 (2006).

[66] J. Lin, Lifshitz transition in two-dimensional spin-density wave models, Phys. Rev. B **82**, 195110 (2010).

[67] J. M. Buhmann and M. Sigrist, Thermoelectric effect of correlated metals: Band-structure effects and the breakdown of Mott's formula, Phys. Rev. B **88**, 115128 (2013).

[68] A. A. Abrikosov, *Fundamentals of the Theory of Metals* (Dover, New York, 1988), pages 111–114.

[69] K. Behnia, D. Jaccard, and J. Flouquet, On the thermoelectricity of correlated electrons in the zero-temperature limit, J. Phys.: Condens. Matter **16**, 5187 (2004).

[70] A. Gourgout, G. Grissonnanche, F. Laliberté, A. Ataei, L. Chen, S. Verret, J.-S. Zhou, J. Mravlje, A. Georges, N. Doiron-Leyraud, and L. Taillefer, Seebeck coefficient in a cuprate superconductor: Particle-hole asymmetry in the strange metal phase and Fermi surface transformation in the pseudogap phase, Phys. Rev. X **12**, 011037 (2022).

[71] S. Nakatsuji and Y. Maeno, Quasi-two-dimensional Mott transition system $Sr_{2-x}Ca_xRuO_4$, Phys. Rev. Lett. **84**, 2666 (2000).

[72] M. Minakata and Y. Maeno, Magnetic ordering in Sr_2RuO_4 induced by nonmagnetic impurities, Phys. Rev. B **63**, 180504(R) (2001).

[73] J. P. Carlo, T. Goko, I. M. Gat-Malureanu, P. L. Russo, A. T. Savici, A. A. Aczel, G. J. MacDougall, J. A. Rodriguez, T. J. Williams, G. M. Luke *et al.*, New magnetic phase diagram of $(Sr, Ca)_2RuO_4$, Nat. Mater. **11**, 323 (2012).

[74] J. E. Ortmann, J. Y. Liu, J. Hu, M. Zhu, J. Peng, M. Matsuda, X. Ke, and Z. Q. Mao, Competition between antiferromagnetism and ferromagnetism in Sr_2RuO_4 probed by Mn and Co doping, Sci. Rep. **3**, 2950 (2013).

[75] B. Zinkl and M. Sigrist, Impurity-induced magnetic ordering in Sr_2RuO_4, Phys. Rev. Res. **3**, 023067 (2021).

[76] N. Kikugawa and Y. Maeno, Non-Fermi-liquid behavior in Sr_2RuO_4 with nonmagnetic impurities, Phys. Rev. Lett. **89**, 117001 (2002).

[77] A. Legros, S. Benhabib, W. Tabis, F. Laliberté, M. Dion, M. Lizaire, B. Vignolle, D. Vignolles, H. Raffy, Z. Z. Li *et al.*, Universal T-linear resistivity and Planckian dissipation in overdoped cuprates, Nat. Phys. **15**, 142 (2019).

[78] C. M. Varma, *Colloquium*: Linear in temperature resistivity and associated mysteries including high temperature superconductivity, Rev. Mod. Phys. **92**, 031001 (2020).

[79] H. Zhao, J. Zhang, M. Lyu, S. Bachus, Y. Tokiwa, P. Gegenwart, S. Zhang, J. Cheng, Y.-f. Yang, G. Chen, Y. Isikawa, Q. Si, F. Steglich, and P. Sun, Quantum-critical phase from frustrated magnetism in a strongly correlated metal, Nat. Phys. **15**, 1261 (2019).

[80] S. Paschen and Q. Si, Quantum phases driven by strong correlations, Nat. Rev. Phys. **3**, 9 (2021).

[81] P. Giannozzi, S. Baroni, N. Bonini, M. Calandra, R. Car, C. Cavazzoni, D. Ceresoli, G. L. Chiarotti, M. Cococcioni, I. Dabo *et al.* QUANTUM ESPRESSO: A modular and open-source software project for quantum simulations of materials, J. Phys.: Condens. Matter **21**, 395502 (2009).

[82] P. Giannozzi, O. Andreussi, T. Brumme, O. Bunau, M. Buongiorno Nardelli, M. Calandra, R. Car, C. Cavazzoni, D. Ceresoli, M. Cococcioni *et al.* Advanced capabilities for materials modelling with Quantum ESPRESSO, J. Phys.: Condens. Matter **29**, 465901 (2017).

[83] P. Giannozzi, O. Baseggio, P. Bonfà, D. Brunato, R. Car, I. Carnimeo, C. Cavazzoni, S. de Gironcoli, P. Delugas, F. Ferrari Ruffino *et al.*, Quantum ESPRESSO toward the exascale, J. Chem. Phys. **152**, 154105 (2020).

[84] M. Kawamura, Y. Gohda, and S. Tsuneyuki, Improved tetrahedron method for the Brillouin-zone integration applicable to response functions, Phys. Rev. B **89**, 094515 (2014).

[85] H.-L. Huang and H.-t. Jeng, Orbital ordering and magnetism in layered perovskite ruthenate Sr_2RuO_4, Sci. Rep. **10**, 7089 (2020).

[86] T. Oguchi, Electronic band structure of the superconductor Sr_2RuO_4, Phys. Rev. B **51**, 1385 (1995).

[87] D. J. Singh, Relationship of Sr_2RuO_4 to the superconducting layered cuprates, Phys. Rev. B **52**, 1358 (1995).

[88] M. W. Haverkort, I. S. Elfimov, L. H. Tjeng, G. A. Sawatzky, and A. Damascelli, Strong spin-orbit coupling effects on the fermi surface of Sr_2RuO_4 and Sr_2RhO_4, Phys. Rev. Lett. **101**, 026406 (2008).

[89] M. Behrmann, C. Piefke, and F. Lechermann, Multiorbital physics in Fermi liquids prone to magnetic order, Phys. Rev. B **86**, 045130 (2012).

[90] Y. J. Sato, A. Nakamura, R. Nishinakayama, R. Okazaki, H. Harima, and D. Aoki, Fermi surface topology and electronic transport properties of chiral crystal $NbGe_2$ with strong electron-phonon interaction, Phys. Rev. B **108**, 235115 (2023).

[91] V. S. Egorov and A. N. Fedorov, Thermopower of lithium-magnesium alloys at the 2 1/2-order transition, Zh. Eksp. Teor. Fiz. **85**, 1647 (1983).